Scaling of local and nonlocal resistances in a 2D topological insulator based on HgTe quantum well

2015 2D Mater. 2 044015

(http://iopscience.iop.org/2053-1583/2/4/044015)

2D Materials

PAPER

Scaling of local and nonlocal resistances in a 2D topological insulator based on HgTe quantum well

A Rahim[1], A D Levin[1], G M Gusev[1], Z D Kvon[2,3], E B Olshanetsky[2], N N Mikhailov[2] and S A Dvoretsky[2]

[1] Instituto de Física da Universidade de São Paulo, 135960-170, São Paulo, SP, Brazil
[2] Institute of Semiconductor Physics, Novosibirsk 630090, Russia
[3] Novosibirsk State University, Novosibirsk, 630090, Russia

E-mail: gusev@if.usp.br

RECEIVED
21 August 2015

REVISED
20 October 2015

ACCEPTED FOR PUBLICATION
29 October 2015

PUBLISHED
16 December 2015

Keywords: two-dimensional systems, topological insulator, HgTe quantum well

Abstract

We report the observation and systematic investigation of a local and nonlocal transport in HgTe quantum wells with inverted band structure corresponding to the two-dimensional topological insulator phase. We examine the probe spacing and probe configuration dependencies of the resistance near the charge neutrality point, where the transport is dominated by edge states. We provide details on the model, which takes into account the edge and bulk contribution to the total current and reproduces our experimental results.

1. Introduction

The two-dimensional topological insulators (2D TI) represent a quantum state of matter with an insulating bulk but gapless one-dimensional states running along the sample edge [1–4]. At the edge electrons with opposite spins propagate in opposite directions thereby forming helical edge states. Systems based on HgTe quantum well are prime candidates for the observation of topological insulator properties in 2D. It has been demonstrated that when the gate voltage variation moves the Fermi level from the bulk electron states to the bulk hole states via the gap with helical edge states, the resistance of HgTe quantum wells shows a broadened peak around the charge neutrality point (CNP) [5, 6]. It was expected that the electrons at the edge of a 2D TI would be protected against the disorder induced scattering and therefore the peak amplitude at the CNP should be approximately equal to $h/2e^2$. Surprisingly, the resistance of samples longer than 1μm was found to be much higher than the quantized value [5, 7]. The lack of the robustness against intrinsic and introduced disorder may be explained by the interaction of the edge states with the electron and hole puddles induced by the spacial potential fluctuations [8].

The observation of a pronounced nonlocal resistance is the main proof of the presence of the edge state transport in a 2D TI. The helical character of the edge state transport makes it possible to describe all resistance measurement configurations within the framework of a resistor network model. In the ballistic transport regime nonlocal resistance has been observed in 6 and 4-probe devices and successfully explained by the Landauer–Büttiker model [9, 10]. Backscattering between helical edge states running along the same boundary in the absence of scattering into the bulk leads to a giant nonlocal resistance peak near the CNP [7, 10–12].

Despite the recent theoretical progress our understanding of the transport properties of 2D topological insulator is far from being complete and further experimental investigations are required. In the case of a pure edge transport we would expect that the nonlocal resistance (R_{NL} could be described within the framework of the resistance network model (conventional Kirchoff's Law). This model predicts that R_{NL} scales linearly with the distance between the contacts along the gated sample edge, rather than the shortest distance between the voltage probes [10]. Comparison of the local and nonlocal resistance for various measurement configurations will allow to determine the average mean free path for the transport via the edge states. Note, however, that a more sophisticated approach is required in order to explore the leakage of current from the edge into the bulk if it exists.

In the present paper we have investigated the nonlocal transport in 6- and 9-probe devices

fabricated on the basis of a 8.3 nm $Cd_{0.65}Hg_{0.35}Te$/HgTe/$Cd_{0.65}Hg_{0.35}Te$ quantum wells. We observe a pronounced nonlocal resistance peak measured in configurations with different distances between the current and voltage probes. We calculate the nonlocal resistance in the presence of scattering between the edge states running along the same boundary and also across the bulk (via the bulk states). In a 2D topological insulator the scattering between helical states running along the same edge is forbidden. However, in a real TI it is assumed, that the edge states coupling may be the result of their interaction with metallic puddles created by the local density fluctuations [8]. Using this model we are able to qualitatively separate the edge-to-edge and edge-to-bulk coupling parameters and describe the local and nonlocal resistance peaks near the CNP.

2. Experiment

Bulk transport in conventional diffusive conductors is governed by the Ohm's law. The resistance of such conductor is directly proportional to its length and inversely proportional to its cross-section, which implies the possibility to describe such transport in terms of a local resistivity or conductivity tensor. The presence of edge states, however, leads to a nonlocal transport which makes the concept of the local resistivity tensor inappropriate. Nonlocal effects appear due to the formation of conducting edge channels that are isolated from the bulk and can carry current to sample regions that would be inaccessible in the case of a conventional diffusive transport. Applying current between a pair of the probes creates a net current along the sample edge and can be detected by another pair of voltage probes away from the dissipative bulk current path. Such nonlocal transport has been observed experimentally in the quantum Hall (QH) systems in the presence of magnetic field and these measurements are now widely acknowledged as constituting definitive experimental evidence for the existence of edge states in the QH regime.

It is worth noting that the physics of the nonlocal transport in the QH and the QSH systems differs significantly. In the QH systems, the nonlocal resistance arises from the suppression of electron scattering between the edge channels and the bulk states. The nonlocality in QSH insulators stems from the unique properties of the helical edge modes in the absence of magnetic field and is an intrinsic characteristic of this novel class of material. In this section we present experimental results of nonlocal transport measurements on two different devices with the following layouts. Device A is a six-probe Hall bar fabricated with a lithographic length 6 μm and width 5 μm (figure 1). Device B specially designed for multi-terminal measurements consists of three narrow (μm wide) consecutive segments of different length (2, 8, 32 μm) and seven voltage probes (see figure 1). The dimensions of gate electrode are 18×10 μm^2 for device A and 62×8 μm^2 for device B. Figure 1(a) shows the local and nonlocal resistance as a function of gate voltage measured for several different configurations in device A. For example, in a local configuration (black line) the current flows between contacts 1–4 and the voltage is measured between contacts pair 2–3; i.e., $R_{I=1-4;V=2-3}$ while in a nonlocal configuration (dotted line) the current flows between contacts 2–6 and the voltage is measured between contacts 2–5, i.e., $R_{I=4-7;V=2-9}$. One can see that the nonlocal signal is three times smaller than the local one. At the same time it is important to mention that both the local and nonlocal resistances are still higher than the resistance quantum h/e^2. The nonlocal signal here is about 70 kOhm, which is four times larger than the resistance quantum.

Figure 1(b) shows the schematic picture of local and nonlocal transport measurements in device B. In local measurements the current is applied between contacts 1–5 and the potential difference is measured between contacts 7–6, 8–7 and 9–8 of the sample. The resulting local resistance is given as $R_{I=1-5;V=9-7}$, $R_{I=1-5;V=8-7}$ and $R_{I=1-5;V=9-8}$ and is shown in figure 1(b) (thick lines). Resistance was also measured in several nonlocal configurations. As an example, consider the configuration when the current is applied between contacts 2–9 (4–7) and the voltage is measured from the contact pairs 3–8(2–9). Schematic drawings in each panel show the measurement configurations. The current probes are indicated by black circles, the voltage probes are indicated by green squares. Again it is worth noting that the nonlocal resistance peaks are narrower as compared to the local resistance peaks measured in the same device.

The figures 2 and 3 summarize the results of the nonlocal resistances measurements for sample B. For clarity we separate different nonlocal configurations. Figure 2 shows the traces for current paths directed perpendicular to the long Hall bar, while figure 3 displays the traces for horizontal current paths.

For a detailed discussion of the nonlocality we concentrate on device B, because the nonlocality could be more conveniently probed in a multiterminal device. This situation can be analyzed by using conventional Kirchoff's law. In this case there is a simple expression that allows one to calculate the resistance value for any measurement configuration assuming that there is only edge state transport in the sample [10]:

$$R^{i,j}_{n,m} = \frac{L_{n,m}L_{i,j}}{lL}\left(h/e^2\right), \qquad (1)$$

where $R^{i,j}_{n,m}$ is the resistance measured between contacts i and j while the current is maintained between contacts n and m, $L_{i,j}$ ($L_{n,m}$) are the distances between i and j (n and m) along the gated sample edge that does not include n and m (i and

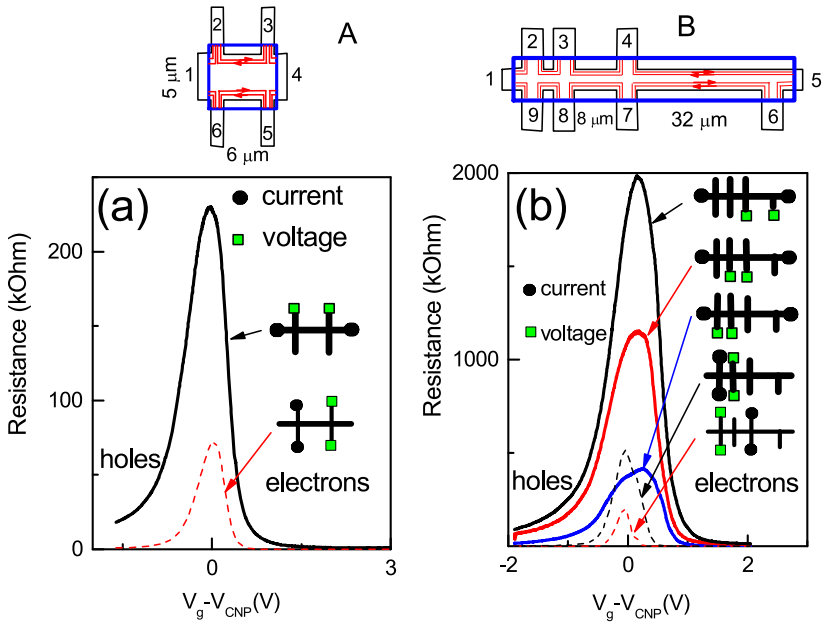

Figure 1. (a) The local and nonlocal resistance R as a function of the gate voltage at zero magnetic field measured from various voltage probes for samples A (a) and B (b), $T = 4.2$ K. Top panel-shows schematic view of the samples. The perimeter of the gate is shown by blue rectangle. Schematic drawings in each panel show the measurement configurations. The current probes are indicated by black circles, the voltage probes are indicated by green squares.

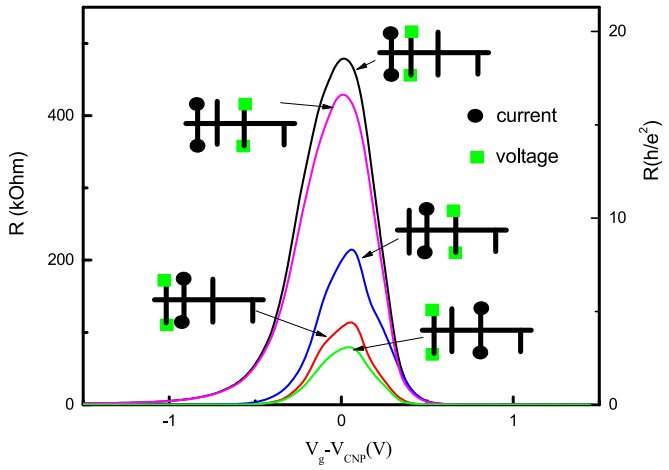

Figure 2. The nonlocal resistance R as a function of the gate voltage at zero magnetic field measured from various voltage probes for sample B, $T = 4.2$ K. Schematics show the measurement configurations. The current flows in the direction perpendicular to the long Hall bar. The current probes are indicated by black circles, the voltage probes are indicated by green squares.

j), L is the total perimeter of the sample, and l is the mean free path. First, we would like to emphasize that the resistance peak value in a conventional local configuration increases linearly with the gated edge length (L_{ij}^{gat}), in agreement with the fact that edge current flows along the gated sample edge. Second, the nonlocal signal is zero when the Fermi level lies deep in the conduction or valence bands and far away from the CNP, and, when the classical model predicts a vanishingly small nonlocal resistance. Finally, when the gate voltage is swept through the CNP the transitions between the edge states and the electron and hole bulk states continue which allows us to study the intermediate situation corresponding to an admixture of the edge and bulk contributions to the conductance.

In order to present our results in a more regular form we collect all experimental data in table 1. Note that equation (1) predicts that the nonlocal resistance near the CNP scales linearly with $L_{i,j}$ or $L_{n,m}$, therefore it is natural to show the data as a function of the distance between the contacts, taking into account the gated edge length. However, as we do not have such a direct proportionality relation, we arrange the data in an ascending order. The table 1 shows the nonlocal peak values near the CNP for different configuration. In the case of a pure edge transport we would expect

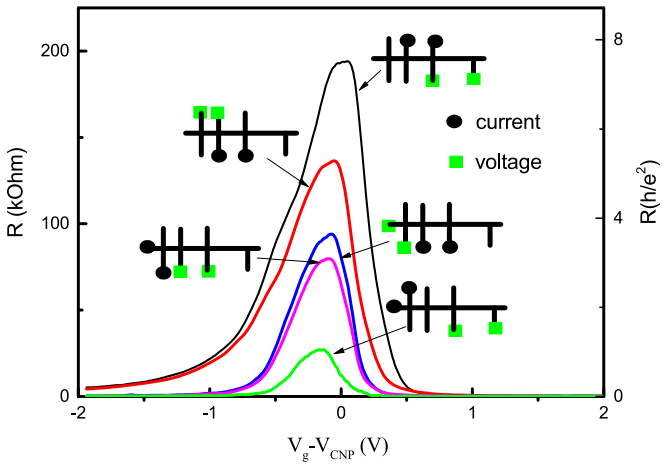

Figure 3. (a) The resistance R curves obtained for another set of nonlocal measuring configurations. These curves are shown separately from those in figure 2 for clarity and to avoid confusion. Schematic drawings show the measurement configurations. The current probes are indicated by black circles, the voltage probes are indicated by green squares.

Table 1. The nonlocal resistance for various configurations obtained for device B compared to the bulk + edge model. The third row represents the mean free path l obtained from the comparison of the experimental results with equation (1), which does not include the bulk contribution (Kirchoff's Law).

Configuration	R_{7-6}^{1-2}	R_{1-9}^{7-8}	R_{2-3}^{7-6}	R_{7-6}^{2-3}	R_{7-8}^{1-9}	R_{7-8}^{1-2}	R_{8-9}^{1-2}	R_{1-9}^{2-3}	R_{3-4}^{1-9}
Experiment (kOhm)	16	20	20	24	68	73	76	96	100
Simulation (kOhm)	7	7	19	22	88	75	40	81	75
Mean free path (μm)	1.88	1.7	2.2	1.9	0.14	0.14	0.13	0.1	0.1
The ratio $\frac{L_{n,m}}{L}$	0.29	0.032	0.048	0.29	0.097	0.097	0.048	0.032	0.097
Configuration	R_{4-7}^{2-9}	R_{1-2}^{3-4}	R_{3-4}^{1-2}	R_{4-7}^{3-8}	R_{3-8}^{4-7}	R_{3-8}^{2-9}	R_{2-9}^{3-8}		
Experiment (kOhm)	100	120	130	210	244	395	450		
Simulation (kOhm)	75	90	97	238	210	426	374		
Mean free path (μm)	1.34	0.08	0.08	1.6	1.3	0.43	0.4		
The ratio $\frac{L_{n,m}}{L}$	0.65	0.032	0.097	0.65	0.13	0.84	0.065		

that the nonlocal resistance could be described within the framework of the resistance network model (conventional Kirchoff's Law). We compare our results with equation (1) and extract the mean free path l, shown in the table 1.

As was expected, the nonlocal resistance cannot be described by a single parameter. The data can be divided in two sets of values-one with $l \approx 2 - 1$ μm and the other with $l \approx 0.4 - 0.1$ μm. As we mentioned above we do not see any clear dependence on the ratio $\frac{L_{n,m}}{L}$. We assume that for an edge current flowing over a long distance there is a high probability for coupling with the bulk states, and the total current experiences large leakage into the bulk. This picture requires a more precise consideration of the bulk contribution.

3. Comparison with bulk-plus-edge model

It has been demonstrated that when the gate voltage variation causes the Fermi level to move from the bulk electron states to the bulk hole states via the gap with helical edge states the resistance of a HgTe quantum well shows a broadened peak around the CNP The peak amplitude is larger than $h/2e^2$. This is surprising because in 2D topological insulator transitions between helical states are forbidden. However, the local density fluctuation may create electron and hole puddles that provide a mechanism for spin flip scattering between helical edge states [8]. Independently of a particular microscopic mechanism responsible for backscattering along the border it can be described by a single phenomenological parameter γ, which is related to the edge–edge scattering rate. The character of the conductivity depends on the position of the Fermi level. When the Fermi energy lies in the conduction or valence bands, the edge states coexist with the bulk states and the mixing between the boundary and the bulk may lead to a strong backscattering. In this case it is important to consider the density of states in order to determine the electron and hole bulk densities and bulk conductivity. Figure 4 shows schematically a simplified profile of the density of states in a HgTe quantum wells. Because of the

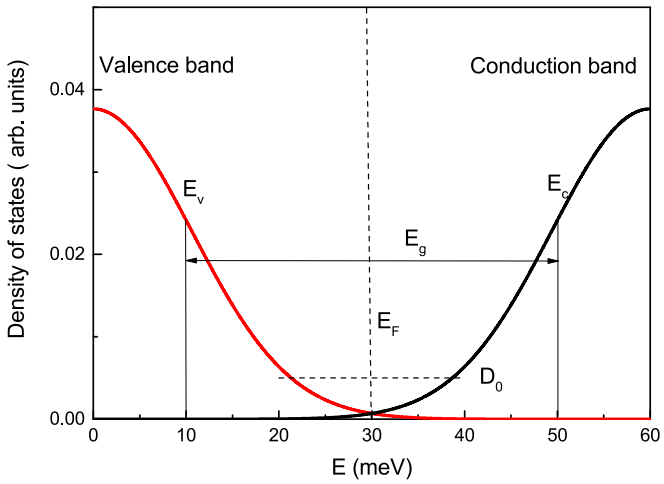

Figure 4. Schematic diagram showing disorder induced smearing of the band edges. Random potential due to the quantum well thickness fluctuations is the cause of the conduction and valence bands having Gaussian tails in the gap. E_v and E_c defines the sharp band edges for an ideal sample in the absence of disorder. The Fermi level E_F is located in the center of the gap. D_0 is the density of the states due to the puddles.

random potential the conduction and valence bands have Gaussian tails stretching into the band gap. According to the generally accepted theory the electrons and holes in the band tails should be localized. However for simplicity we assume a finite residual conductivity in the band tails in order to explain the reduction of nonlocal transport near the CNP. The scattering between the edge states and the bulk can be described by a phenomenological parameter g, which is related to the edge-bulk scattering rate.

The local and nonlocal transport coefficients arise from the edge state contribution and the short-circuiting of the edge transport by the bulk contribution, the latter being more important away from the CNP. Below we reproduce the basic features of this model [7, 13]. The transport properties in the bulk can be described by the current–voltage relation

$$\mathbf{j}_i(\mathbf{r}) = -\hat{\sigma}_i \nabla \psi_i(\mathbf{r}),$$
$$\hat{\sigma}_i = \begin{pmatrix} \sigma_{xx}^{(i)} & \sigma_{xy}^{(i)} \\ \sigma_{yx}^{(i)} & \sigma_{xx}^{(i)} \end{pmatrix}, \quad (2)$$

where $i = 1, 2$ labels the states with different projections of the spin, ψ_i are the electrochemical potential for electrons, and $\mathbf{r} = (x, y)$ is the 2D coordinate. Since we consider isotropic conduction, the nondiagonal part of the conductivity tensor appears only in a nonzero magnetic field. Assuming the components of the conductivity tensor to be coordinate-independent parameters, we can solve the problem by solving the Laplace equation for the potentials, $\nabla^2 \psi_i(\mathbf{r}) = 0$, because the charge conservation law and the continuity conditions require $\nabla \mathbf{j}_i(\mathbf{r}) = 0$. The solution to the Laplace equation is fully determined by the boundary conditions, which in our case are modified by the bulk-edge current leakage. In order to describe the transport in the presence of the edge states, we introduce two phenomenological constants γ and g, which represent edge to edge and bulk to edge inverse scattering length, respectively. Then, the boundary conditions corresponding to a zero current normal to the boundary in the presence of a bulk-edge coupling are given by

$$\mathbf{n}\mathbf{j}_i = g\left(\psi_i - \varphi_i\right), \quad (3)$$

where φ_i are the local chemical potentials of the edge states, ψ_i and $\mathbf{j}_i$ are the potentials and currents at the boundary, and $\mathbf{n}$ is a unit vector normal to the boundary.

The edge state transport can be described by the continuity equations [13, 14] taking into account the scattering between the edge and the bulk:

$$\partial_x \varphi_1 = \gamma(\varphi_2 - \varphi_1) + g\left(\psi_1 - \varphi_1\right), \quad (4)$$

$$-\partial_x \varphi_2 = \gamma(\varphi_1 - \varphi_2) + g\left(\psi_2 - \varphi_2\right). \quad (5)$$

The general solution of this problem, therefore, includes the solution of a 2D Laplace equation for the bulk electrochemical potentials $\psi_{1,2}(x, y)$ together with equations (2)–(4) describing the scattering between the edge states and between the edge and the bulk states. The current can be calculated from this solution as a sum of the contributions from the bulk and the edge states. In nonlocal configurations the edge + bulk model can be solved only numerically. We have performed self-consistent calculations to find the $\psi_{1,2}$ solution of the Laplace equation in 2D and the $\varphi_{1,2}$ solutions of equations (3) and (4) on the edge using the Hall bar geometry schematically shown in figure 1. The contacts are assumed to be thermal reservoirs, where a full mixing of electron spin states and bulk states occurs [14]. Note that, in contrast to the standard QHE, where the mixing of the edge states occurs within the metallic Ohmic contacts, in our samples the mixing will take place in the parts of the sample that lie outside of the metallic gate and contain 2D electron gas.

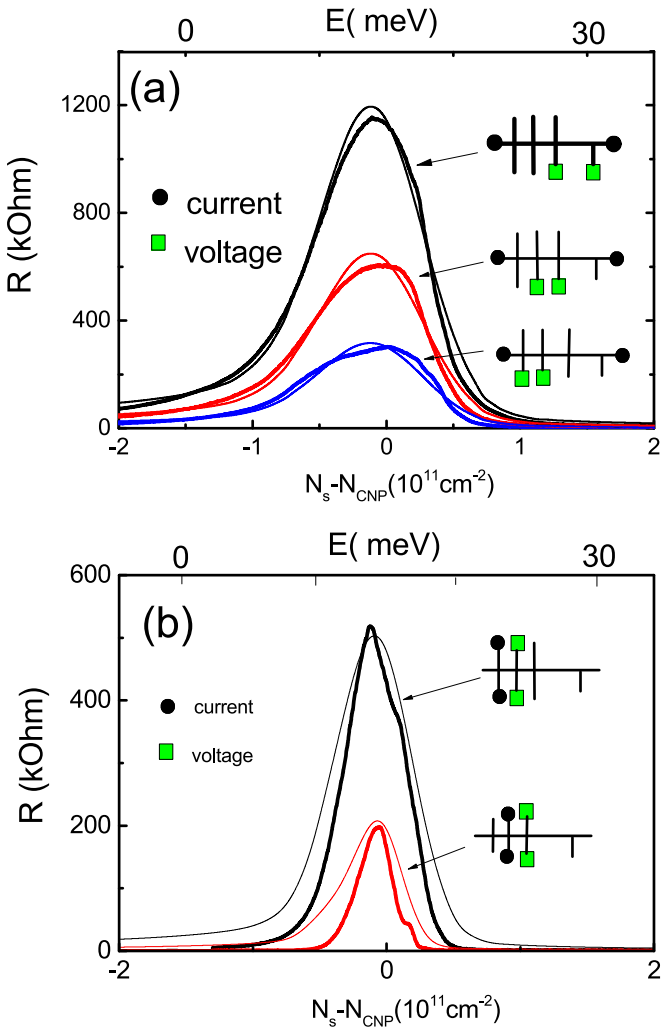

Figure 5. (a) Comparison of local resistances for three segments of device B. Thin traces show resistances for all the three segments predicted by the edge + bulk transport model. (b) Nonlocal resistances for two different measurement configurations of device B. The red solid line is the nonlocal resistance when the current is applied between contacts 2–9 and the potential is measured between 3–8. The blue solid line represents the nonlocal signal when the current is applied between contacts 4–7 and voltage is measured between contacts 2–9. The thin traces are the corresponding signals predicted by the theory.

The equations for $\psi_{1,2}$ are discretized by the finite element method. The generalized Neumann boundary conditions, equation (2), are set in the regions outside the metal contacts. To solve the boundary value problem for a system of ordinary differential equations (3) and (4) we use a finite difference code that implements the 3-stage Lobatto IIIa formula. The boundary conditions inside the metal contacts are set to $\varphi_{1,2} = \psi_{1,2}$.

Both in local and nonlocal configurations the resistance is calculated as

$$R_{xx} = V\ I_{\rm tot}^{-1},\ \ I_{\rm tot} = I_{\rm edge} + I_{\rm bulk},$$
$$V = \frac{1}{2}\left(\varphi_{11} - \varphi_{11'} + \varphi_{21} - \varphi_{21'}\right), \qquad (6)$$

where V is the potential difference at the voltage probes, $I_{\rm tot}$ is the total current flowing between the current contacts, φ_{i1} and $\varphi_{i1'}$ are the potentials at the voltage probe locations. The edge and bulk currents for the local case (at an arbitrary point x along the sample) are given by

$$I_{\rm edge} = \frac{e^2}{h}\left(\varphi_1 - \varphi_2 + \varphi_{2'} - \varphi_{1'}\right),$$
$$I_{\rm bulk} = \sum_{i=1,2}\left[\sigma_{xy}^{(i)}\left(\psi_i - \psi_{i'}\right) - \sigma_{xx}^{(i)}\int {\rm d}y\frac{\partial\psi_i}{\partial x}\right], \qquad (7)$$

where φ_i, ψ_i and $\varphi_{i'}$, $\psi_{i'}$ are the potentials at the opposite (bottom and top, respectively) edges of the sample, and the integral is taken across the sample from bottom to top. For nonlocal case the currents are calculated from similar expressions:

$$I_{\rm edge} = \frac{e^2}{h}\left(\varphi_1 - \varphi_2 + \varphi_{2'} - \varphi_{1'}\right),$$
$$I_{\rm bulk} = \sum_{i=1,2}\left[\sigma_{yx}^{(i)}\left(\psi_i - \psi_{i'}\right) - \sigma_{xx}^{(i)}\int {\rm d}x\frac{\partial\psi_i}{\partial y}\right], \qquad (8)$$

where now φ_i, ψ_i and $\varphi_{i'}$, $\psi_{i'}$ are the potentials at the opposite (left and right, respectively) edges of the current contact, and the integral is taken across this current contact from left to right. The conductivities are calculated as $\sigma_{xx}^{(1)} = \sigma_{xx}^{(2)} = {\rm e}(\mu_n n + \mu_p p)/2$,

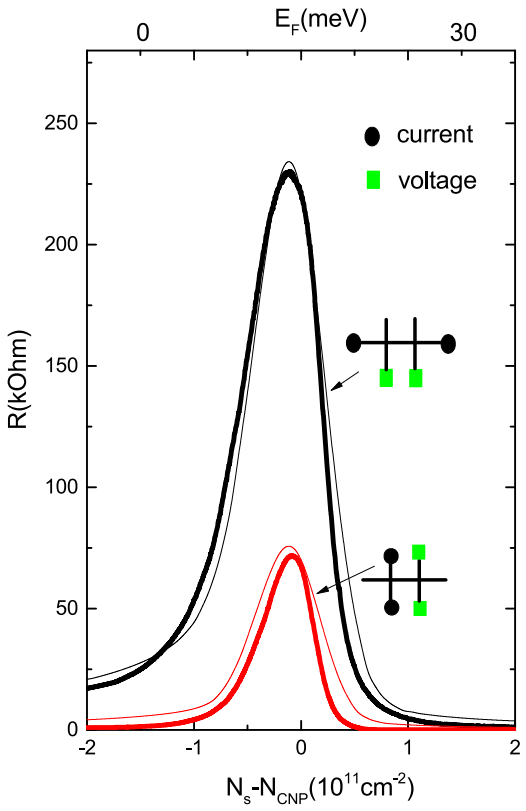

Figure 6. Comparison of local resistances for device A. Thin traces show resistances predicted by the edge + bulk transport model.

where μ_n and n (μ_p and p) are electron (hole) mobilities and densities. To find n and p, the bulk densities of states for electrons and holes are represented by steps $D_{n,p} = 4\pi m_{n,p}/h^2$ with $m_{n,p}$ being the effective masses of electrons and holes. The energy gap separating electron and hole bands is $E_g = 30$ meV. In addition, the sharp band edges are smeared according to the Gaussian law with the broadening energies $\Gamma_{n,p} = \hbar/\tau_{n,p}$, where $\tau_{n,p} = \mu_{n,p} m_{n,p}/e$. The following parameters have been used: $\mu_n = 80\,000$ cm^2 V^{-1} s^{-1}, $\mu_p = 5000$ cm^2 V^{-1} s^{-1}, $m_n = 0.024\, m_0$, $m_p = 0.15\, m_0$, where m_0 is the free electron mass. The extended states are separated by a mobility gap ~1 meV. The comparison shown in figures 5 and 6 and is the representative behavior of a couple of local and nonlocal measurement configurations in devices A and B respectively. The best agreement between the experiment and theory is reached for the value of phenomenological parameters $\gamma = 3.0\ \mu$m^{-1} and $g = 0.03\ \mu$m^{-1} for the sample A. For device B we obtain $\gamma = 1.4\ \mu$m^{-1} and $g = 0.05\ \mu$m^{-1}. The comparison of the experimental and simulated values of the nonlocal resistance peaks near the CNP for sample B is given in table 1. One may see that the agreement between the calculations and the experimental data is much better than in the case of the Kirchoff's network model. It is worth noting that all 17 values of the nonlocal resistance are satisfactorily described by only two adjustable parameters. Indeed all the local resistance values (six possible configurations) also agree with calculations. Better agreement with edge + bulk model strongly supports the existence of the scattering into the bulk. near CNP.

In the rest of the paper we would like to discuss the dependence of the nonlocal resistance on the density. Our model is much too simple to adequately describe the shape of the resistance peaks, shown in figures 5 and 6. The model reproduces the key feature of the nonlocal resistance, for example, a faster than in the case of a local resistance suppression of the peak away from CNP which is the result of a short-circuiting of the edge transport by the bulk contribution. However, we can not directly translate the energy dependence to the density dependence, because the Fermi energy does not vary linearly with N_s in the bulk gap region. In the absence of disorder the Fermi level jumps from the conduction to the valence band, and a sharp resistance peak is expected, in contrast to the broad maximum observed in the experiment. The existence of the metallic puddles can be responsible for a smoother Fermi level displacement [15]. For simplicity's sake we can assume that the fraction of the metallic coverage of the sample is constant, which leads to a constant density of states inside of the bulk gap D_0 (figure 4). Comparing the energy and the density scales in figures 5 and 6 we obtain $D_0 = 5 \times 10^{10}$ cm^{-2} meV^{-1} which is close to the density of states of the electrons in the conduction band. We may assume that the metallic coverage $p < 0.5$ is still below the percolation threshold and electrons are localized. Therefore, coexistence of the localized and delocalized electrons is needed for the description of the transport in a 2D TI. The localized electrons are responsible for a continuous transition of the Fermi level through the bulk gap, while delocalized carriers are responsible for a weak suppression of the nonlocal signal near the CNP and a its strong suppression away from the CNP. While our experiment offers an interesting outlook on the edge and bulk transport in a 2D TI, more experimental and theoretical work is required to understand the behavior of 2D electron system in such complex objects as disordered HgTe quantum wells.

Acknowledgments

The work was supported by the RFBI Grant No. N15-02-00217-a, by FAPESP CNPq (Brazilian agencies) and by TWAS-CNPq.

References

[1] Hasan M Z and Kane C L 2010 *Rev. Mod. Phys.* **82** 2045
Qi X-L and Zhang S-C 2011 *Rev. Mod. Phys.* **83** 1057
[2] Qi X-L and Zhang S-C 2010 *Phys. Today, Phys. Today* **63** 33
[3] Moore J E and Balents L 2007 *Phys. Rev.* B **75** 121306
[4] Moore J E 2010 *Nature* **464** 194
[5] König M, Wiedmann S, Brune C, Roth A, Buhmann H, Molenkamp L W, Qi X-L and Zhang S-C 2007 *Science* **318** 766
[6] Buhmann H 2011 *J. Appl. Phys.* **109** 102409

[7] Gusev G M, Kvon Z D, Shegai O A, Mikhailov N N, Dvoretsky S A and Portal J C 2011 *Phys. Rev.* B **84** 121302(R)
[8] Vayrynen J I, Goldstein M and Glazman L I 2013 *Phys. Rev. Lett.* **110** 216402
[9] Roth A, Brüne C, Buhmann H, Molenkamp L W, Maciejko J, Qi X-L and Zhang S-C 2009 *Science* **325** 294
[10] Olshanetsky E B, Kvon Z D, Gusev G M, Levin A D, Raichev O E, Mikhailov N N and Dvoretsky S A 2015 *Phys. Rev. Lett.* **114** 126802
[11] Gusev G M, Olshanetsky E B, Kvon Z D, Mikhailov N N and Dvoretsky S A 2013 *Phys. Rev.* B **87** 081311(R)
[12] Gusev G M, Kvon Z D, Olshanetsky E B, Levin A D, Krupko Y, Portal J C, Mikhailov N N and Dvoretsky S A 2014 *Phys. Rev.* B **89** 125305(R)
[13] Abanin D A, Novoselov K S, Zeitler U, Lee P A, Geim A K and Levitov L S 2007 *Phys. Rev. Lett.* **98** 196806
[14] Dolgopolov V T, Kravchenko G V and Shashkin A A 1991 *Solid State Commun.* **78** 999
[15] Gusev G M, Olshanetsky E B, Kvon Z D, Raichev O E, Mikhailov N N and Dvoretsky S A 2013 *Phys. Rev.* B **88** 195305